A checkerboard-free symmetry-preserving conservative method for magnetohydrodynamic flows

J A Hopman, F X Trias and J Rigola

Heat and Mass Transfer Technological Center, Technical University of Catalonia, ESEIAAT, c/Colom 11, 08222 Terrassa, Spain,

E-mail: jannes.hopman@upc.edu

Abstract. Simulating MHD flows at high Hartmann numbers and low magnetic Reynolds numbers is of high interest for the design of a nuclear fusion breeding blanket, for which high accuracy and conservation of physical properties are of great importance. In this work, a solver is developed that offers these properties through the symmetry-preserving method, while at the same time warranting unconditional stability. Since this method uses predictor values for the pressure and electric potential fields, it can be prone to checkerboarding. Therefore it is extended to include a dynamical checkerboarding solution, which balances this problem with numerical dissipation. This is done through run-time measurements of the intensity of checkerboarding, which is then used as a negative feedback onto the predictor values. The symmetry-preserving discretisation and the dynamical solution to checkerboarding were successfully tested using an magnetohydrodynamic Taylor-Green vortex. The newly introduced method shows results free from numerical dissipation in smooth cases, whereas it avoids checkerboarding in more challenging cases. Finally, the method shows to be unconditionally stable, even on highly distorted meshes.

1. Introduction

Studying magnetohydrodynamic (MHD) flows is of great interest in the development of a nuclear fusion reactor, since the required tritium is obtained through liquid metal breeding blankets inside the reactor. The strong magnetic field which contains the reaction plasma inside the core interacts with this liquid metal creating complex flow phenomena [1]. Some of the main challenges in simulating MHD flows concern [2]: (i) Properly discretising the flow variables and operators, to accurately depict the delicate balance between the pressure drop and the opposing generated Lorentz force, which is especially difficult in complex geometries. (ii) In fusion reactor settings, the induction-less approximation can be made leading to a second Poisson equation, increasing computational cost of the simulation. (iii) Code validation can be difficult, since experimental set-up and measurement are often impossible.

Applying the symmetry-preserving method, in which properties of the discrete operators reflect their continuous counterparts, ensures conservation of physical properties, such as mass, momentum, kinetic energy and current density [3]. With this method, the delicate force balance is not disrupted by numerical dissipation and neither is the transition from laminar to turbulent regions, while unconditional stability is warranted simultaneously. This method was extended to collocated grid arrangements by [4], and the electromagnetic terms were added by [5].

For collocated grid arrangements, the checkerboard problem can arise, caused by a pressure decoupling between neighbouring cells if they are calculated using central differencing schemes for the discrete operators. A common way to avoid this problem is by employing a weighted interpolation method (WIM) of which the pressure-weighted interpolation is the most well-known [6]. This method can be combined with the use of a compact-stencil Laplacian, which reduces computational complexity and is therefore often favoured by industrial codes. The WIM has been extended to include other terms such as relaxation factors and transient terms [7], but it inadvertently introduces a numerical error. The order of the pressure error that is introduced by employing a WIM and a compact-stencil Laplacian can be reduced by adding a pressure gradient in the momentum predictor [8]. Although this method reduces numerical dissipation, it can reintroduce checkerboarding to the results, even while using the WIM and a compact-stencil Laplacian [9]. By quantifying the checkerboarding intensity during run-time, and using it as a negative feedback on the use of a pressure predictor, numerical dissipation and checkerboarding were succesfully balanced by [10].

Since the method of [5] includes a second Poisson equation for the electric potential, which can lead to checkerboarding as well, it is of interest to apply the same method to both the hydrodynamic and the electromagnetic parts of the algorithm. This method was implemented in OpenFOAM as an extension of the *RKSymFoam* code of [9, 11]. This method is described in section 2 and tested using an MHD Taylor-Green vortex in section 3. Finally, conclusions of the work are drawn and future considerations are given in section 4.

2. Numerical methods

In fusion reactor settings, flows have a small magnetic Reynolds number, $Re_m = \sigma\mu L u_0 \ll 1$, with σ, μ, L and u_0 indicating the conductivity, magnetic permeability, characteristic length and characteristic velocity, respectively. In this case, the induction-less approximation can be made, which states that the imposed magnetic field is not affected by the flow. The following set of equations then govern the MHD flow:

$$\frac{\partial \mathbf{u}}{\partial t} + (\mathbf{u}\cdot\nabla)\,\mathbf{u} = \nu\nabla^2\mathbf{u} - \nabla\,(p/\rho) + (\mathbf{J}\times\mathbf{B})\,/\rho, \qquad \nabla\cdot\mathbf{u} = 0, \tag{1}$$

$$\mathbf{J} = \sigma\,(-\nabla\phi + \mathbf{u}\times\mathbf{B})\,, \qquad \nabla\cdot\mathbf{J} = 0. \tag{2}$$

with velocity ($\mathbf{u}$), time (t), kinematic viscosity (ν), pressure (p), density (ρ), current density ($\mathbf{J}$), magnetic field ($\mathbf{B}$) and electric potential (ϕ). The hydrodynamic part is treated using the classical projection method, and for the electromagnetic part a second Poisson equation can be derived from equation (2) as:

$$\nabla^2\phi = \nabla\cdot(\mathbf{u}\times\mathbf{B})\,. \tag{3}$$

These equations are implemented in an algorithm, based on the work of [12, 13], adjusted to the symmetry-preserving method and notation of [4], as follows:

$$\mathbf{u}_c^p = \mathbf{u}_c^n - \Delta t\Omega^{-1}\left(C\left(\mathbf{u}_s^n\right) + D\right)\mathbf{u}_c^n - \theta_p\Gamma_{sc}G\tilde{\mathbf{p}}_c^n + N[\mathbf{J}_c^n]_\times\mathbf{B}_c^n, \tag{4a}$$

$$\mathbf{u}_s^p = \Gamma_{cs}\mathbf{u}_c^p, \tag{4b}$$

$$L\tilde{\mathbf{p}}_c' = M\mathbf{u}_s^p, \tag{4c}$$

$$\mathbf{u}_s^{n+1} = \mathbf{u}_s^p - G\tilde{\mathbf{p}}_c', \tag{4d}$$

$$\mathbf{u}_c^{n+1} = \mathbf{u}_c^p - \Gamma_{sc}G\tilde{\mathbf{p}}_c', \tag{4e}$$

$$\tilde{\mathbf{p}}_c^{n+1} = \theta_p\tilde{\mathbf{p}}_c^n + \tilde{\mathbf{p}}_c', \tag{4f}$$

$$\mathbf{J}_c^p = [\mathbf{u}_c^{n+1}]_\times\mathbf{B}_c^{n+1} - \theta_\phi\Gamma_{sc}G\boldsymbol{\phi}_c^n, \tag{4g}$$

$$\mathbf{J}_s^p = \Gamma_{cs}\mathbf{J}_c^p, \tag{4h}$$

$$L\boldsymbol{\phi}_c' = M\mathbf{J}_s^p, \tag{4i}$$

$$\mathbf{J}_c^{n+1} = \Gamma_{sc}\left(\mathbf{J}_s^p - G\boldsymbol{\phi}_c'\right), \tag{4j}$$

$$\boldsymbol{\phi}_c^{n+1} = \theta_\phi\boldsymbol{\phi}_c^n + \boldsymbol{\phi}_c', \tag{4k}$$

with interaction parameter $N = \frac{Ha^2}{Re} = \frac{B_0^2 L \sigma_0}{u_0 \rho_0}$, giving a ratio between the Reynolds number, $Re = \frac{u_0 L}{\nu}$, and the Hartmann number, $Ha = LB_0\sqrt{\frac{\sigma_0}{\rho_0 \nu}}$, in which subscript 0 indicates a characteristic value. θ_p and θ_ϕ are scalar values to control use of a gradient value in the predictor equations. $[A]_\times$ denotes the cross-product form of vector A.

One notable difference with the algorithm by [12, 13] is the use of a volumetric cell-to-face interpolator, Γ_{cs}, throughout the algorithm, which has been shown to be conservative and unconditionally stable [14]. Its symmetry-preserving counterpart, the face-to-cell interpolator, is expressed as:

$$\Gamma_{sc} = \Omega^{-1}\Gamma_{cs}^T\Omega_s, \tag{5}$$

which is a necessary property of the symmetry-preserving method. In contrast, the interpolator of equation (4j) in the method of [12, 13] is given by:

$$\left[\Gamma_{sc}^{Ni}\alpha_s\right]_c = \sum_f \frac{A_f\left(\mathbf{r}_f - \mathbf{r}_c\right)}{\Omega_c}[\alpha_s]_f, \tag{6}$$

which is not strictly dissipative on non-circumcenter meshes, as equation (5) does not hold.

The other novelty in the algorithm of equation (4), is the addition of θ_p and θ_ϕ. By quantifying the checkerboarding of the $\mathbf{p}_c$ and $\boldsymbol{\phi}_c$ fields, these scalar coefficients can be used to enforce the negative feedback on the usage of predictor values for the respective equations. This quantification method was derived by [10] as:

$$\theta_a = \frac{a_c^T L_c a_c}{a_c^T L a_c}, \tag{7}$$

in which $L_c = M_c G_c = M\Gamma_{cs}\Gamma_{sc}G$ and L give the wide-stencil and compact-stencil Laplacian operators, respectively. $\theta_a \in [0, 1]$ gives a global, normalised, non-dimensional, time-step independent coefficient for the intensity of checkerboarding of field a_c.

A symmetry-preserving algorithm with the interpolation of equation (4j) given by equation (6) is compared to the algorithm of equation (4), using static and dynamic values for θ_p and θ_ϕ. An overview of the solvers is given below:

Table 1. Settings of the tested solvers

	SP-θ_0	SP-θ_1	SP-θ_{dy}	Ni
Γ_{sc}	Eq.(5)	Eq.(5)	Eq.(5)	Eq.(6)
θ_p	0	1	Eq.(7)	1
θ_ϕ	0	1	Eq.(7)	0

3. Results

An MHD Taylor-Green vortex was designed from the hydrodynamic case which consists of four vortices on a square domain with $0 \leq x \leq 2\pi$, $0 \leq y \leq 2\pi$ and cyclic boundaries, to which non-zero conductivity σ_0 and a magnetic field $\mathbf{B} = (0, 0, B_z)$ are introduced. The analytical solutions of the main solution variables, in non-dimensional units, are given by:

$$u_x(x, y, t) = \sin(x)\cos(y)e^{-2\nu t}, \tag{8}$$

$$u_y(x, y, t) = -\cos(x)\sin(y)e^{-2\nu t}, \tag{9}$$

$$p(x, y, t) = \frac{1}{4}(\cos(2x) + \cos(2y))e^{-4\nu t}, \tag{10}$$

$$\phi = -\cos(x)\cos(y)B_z e^{-2\nu t}. \tag{11}$$

The additional electric potential field generates a current which exactly cancels the current induced by the magnetic field, such that $\mathbf{u} \times \mathbf{B} = \nabla\phi$:

$$\mathbf{u} \times \mathbf{B} = \begin{pmatrix} -\cos(x)\sin(y)B_z e^{-2\nu t} \\ -\sin(x)\cos(y)B_z e^{-2\nu t} \\ 0 \end{pmatrix} = \nabla\phi. \tag{12}$$

The levels of checkerboarding were monitored using equation (7). Additionally, the accuracy of the methods was measured using the kinetic energy budgets, given by [15]:

$$\begin{aligned} &\partial_t E_k && \text{Evolution,} \\ =& -\mathbf{u}\cdot((\mathbf{u}\cdot\nabla)\,\mathbf{u}) && \text{Transport,} \\ &-\mathbf{u}\cdot(\nabla p)/\rho && \text{Pressure diffusion,} \\ &+\nu\nabla^2 E_k && \text{Viscous diffusion,} \\ &-\nu\,(\nabla\mathbf{u}) : (\nabla\mathbf{u}) && \text{Dissipation,} \\ &+\mathbf{u}\cdot(\mathbf{J}\times\mathbf{B})/\rho, && \text{Lorentz force term,} \end{aligned}$$

where $E_k(t) = \frac{\mathbf{u}\cdot\mathbf{u}}{2}$, which for the analytical case is given by $E_{ana}(t) = E_k(0)e^{-4\nu t}$. Since the induced currents should cancel out, all terms should equal zero globally, except the dissipation term which depends on ν, given analytically by $-4\nu E_k(0)e^{-4\nu t}$. In practice, the transport term equals zero due to skew symmetry of the convective operator and the viscous diffusion term equals zero since each face term cancels itself in a global divergence calculation, therefore they are no further considered. For budget term B_{num}, the numerical error is then expressed as:

$$\epsilon_{num} = \frac{B_{num} - B_{ana}}{E_k}. \tag{13}$$

This set-up was tested for the solvers given in table 1, on meshes with different levels of deformation, as seen in figure 1. The case was run with zero viscosity and with $Re = \frac{u_0 L}{2\pi\nu} = 100$, and for the latter case, the Hartmann number was set to $Ha = \frac{L}{2\pi}B_z\sqrt{\frac{\sigma_0}{\rho\nu}} \in \{0, 100\}$.

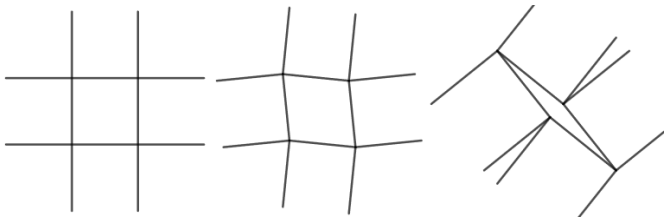

Figure 1. Mesh deformation levels. Left: Uniform. Center: Perturbed. Right: Distorted.

Figure 2a shows that for the inviscid case on a uniform grid, the numerical dissipation is very low. SP-θ_0 shows the pressure error which remains. The lack of checkerboarding, seen in table 2, causes SP-θ_{dy} to converge to SP-θ_1. Figure 2b shows that introduction of viscosity causes a numerical error in each case, because of under-estimation of the dissipation term. These errors do not cause any problems, due to their magnitude and the fact that, overall, energy is still dissipated. Introduction of the magnetic field, as seen in figure 2c shows that for all cases on a uniform mesh, the current density is conserved, with a small deviation in SP-θ_0, caused most probably by similar mechanisms as the pressure error in figure 2a. Up until this point, no significant checkerboarding has been measured in any of the cases or fields, and SP-θ_{dy} has

converged to SP-θ_1 every time. When the mesh gets perturbed, however, the SP-θ_1 method becomes prone to checkerboarding and as a result, SP-θ_{dy} removes the pressure prediction in equation 4a and converges to SP-θ_0 instead, favouring a smooth solution at the cost of some numerical dissipation. At the same time, it can be seen that the Ni interpolation method loses its conservative properties, as was predicted in section 2.

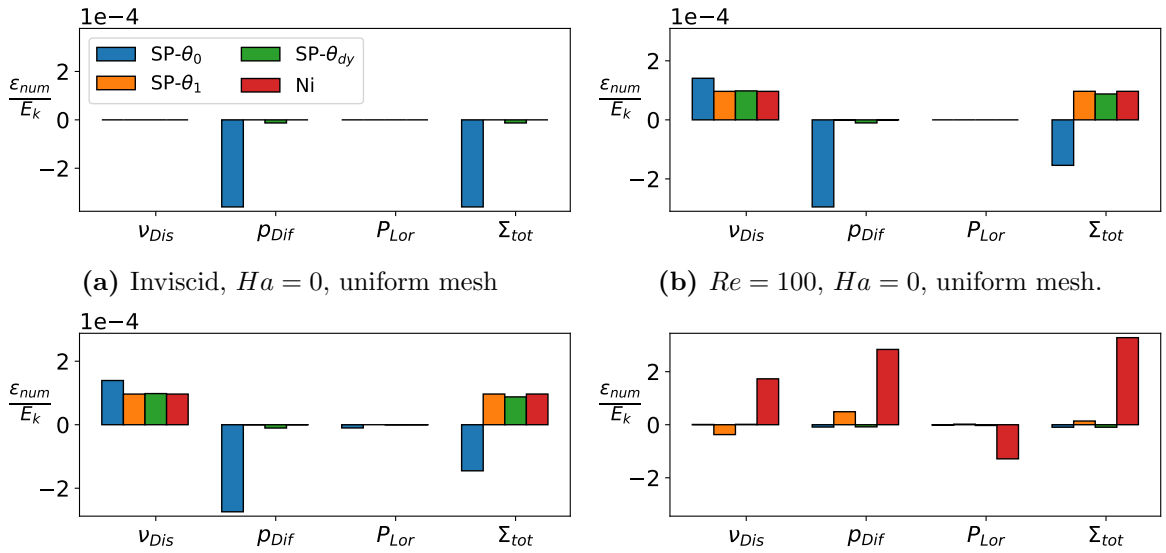

(a) Inviscid, $Ha = 0$, uniform mesh

(b) $Re = 100$, $Ha = 0$, uniform mesh.

(c) $Re = 100$, $Ha = 100$, uniform mesh

(d) $Re = 100$, $Ha = 100$, perturbed mesh.

Figure 2. Kinetic energy budgets in a Taylor-Green vortex.

Moreover, if the deformation of the mesh is pushed to an extreme, it can be seen from figure 3 that this method quickly diverges. Methods SP-θ_0 and SP-θ_{dy} show severe over-dissipation, however they remain stable, whereas SP-θ_1 also shows a slow divergence due to accumulation of kinetic energy. These results show that SP-θ_{dy} benefits from the low order pressure error in smooth cases, but does not have the drawback of SP-θ_1 when a field is prone to checkerboarding. At the same time, the combination with the interpolation of (5) provides unconditional stability.

Table 2. Checkerboard coefficients for pressure and electric potential in a Taylor-Green vortex

			SP-θ_0		SP-θ_1		SP-θ_{dy}		Ni	
Re	Ha	Mesh	p_{cb}	ϕ_{cb}	p_{cb}	ϕ_{cb}	p_{cb}	ϕ_{cb}	p_{cb}	ϕ_{cb}
Inviscid	0	uniform	0.04	-	0.04	-	0.04	-	0.04	-
100	0	uniform	0.04	-	0.04	-	0.04	-	0.04	-
100	100	uniform	0.04	0.01	0.04	0.01	0.04	0.01	0.04	0.01
100	100	perturbed	0.83	0.01	1.00	0.89	0.85	0.01	1.00	0.05

4. Conclusions and outlook

A checkerboard-free symmetry-preserving method for MHD flows has been introduced in this work and the initial tests show promising results. Integrating the dynamic predictor values for the pressure and electric potential fields, by quantifying checkerboarding and using it as negative feedback, shows that the solver can be free from numerical dissipation in smooth cases, while at the same time free from checkerboarding in cases that are prone to this problem.

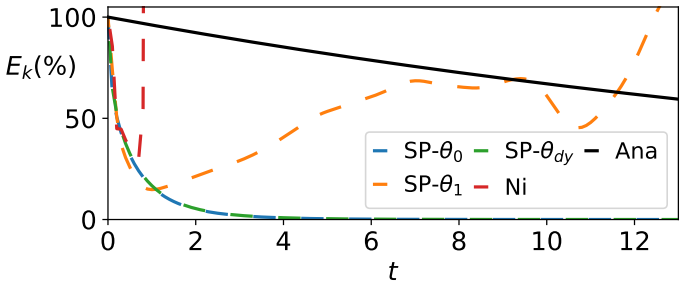

Figure 3. Kinetic energy over time in a Taylor-Green vortex on the distorted mesh.

This method is proven to be even more useful in MHD setting where an additional Poisson equation has to be solved. Moreover, the symmetry-preserving discretisation eliminates any significant numerical dissipation, and, when combined with the dynamic predictor values, shows unconditional stability.

To further validate this method, additional laminar benchmark tests will be performed to demonstrate its high accuracy and stability, while simultaneously avoiding solutions with checkerboarding, even on unstructured meshes. In addition to this, turbulent MHD cases will be used to show that the energy-preserving properties should accurately predict higher-order statistics and transition regimes.

Acknowledgments

This work is supported by the SIMEX project (PID2022-142174OB-I00) of *Ministerio de Ciencia e Innovación*, Spain and the RETOtwin project (PDC2021-120970-I00) of *Ministerio de Economía y Competitividad*, Spain. J.A.H. is supported by the predoctoral grant FI 2023 (2023 FI_B1 00204) of the *Catalan Agency for Management of University and Research Grants (AGAUR)*.

References

[1] Abdou M *et al.* 2001 *Fusion Eng. Des.* **54** 181–247
[2] Smolentsev S *et al.* 2015 *Fusion Eng. Des.* **100** 65–72
[3] Verstappen R and Veldman A 2003 *J. Comput. Phys.* **187** 343–368
[4] Trias F X, Lehmkuhl O, Oliva A, Pérez-Segarra C D and Verstappen R 2014 *J. Comput. Phys.* **258** 246–267
[5] Hopman J A, Trias Miquel F X and Rigola Serrano J 2022 *Proc. ECCOMAS8*
[6] Rhie C M and Chow W L 1983 *AIAA J.* **21** 1525–1532
[7] Bartholomew P, Denner F, Abdol-Azis M H, Marquis A and van Wachem B G 2018 *J. Comput. Phys.* **375** 177–208
[8] Van Kan J 1986 *SIAM J. Sci. Comput.* **7** 870–891
[9] Komen E M, Hopman J A, Frederix E, Trias F X and Verstappen R W 2021 *Comput. Fluids* **225** 104979
[10] Hopman J, Alsalti-Baldellou A, Trias F X and Rigola J 2023 *Proc. THMT23*
[11] Hopman J and Frederix E 2023 RKSymFoam GitHub repository accessed on January 22, 2024
[12] Ni M J, Munipalli R, Morley N B, Huang P and Abdou M A 2007 *J. Comput. Phys.* **227** 174–204
[13] Ni M J, Munipalli R, Huang P, Morley N B and Abdou M A 2007 *J. Comput. Phys.* **227** 205–228
[14] Santos D, Trias F X, Hopman J and Pérez-Segarra C 2023 *Proc. THMT23*
[15] Durbin P A and Reif B P 2011 *Statistical theory and modeling for turbulent flows* (John Wiley & Sons)